How Significant Was the 1877/78 El Niño?

BOYIN HUANG

NOAA/National Centers for Environmental Information, Asheville, North Carolina

MICHELLE L'HEUREUX AND ZENG-ZHEN HU

NOAA/Climate Prediction Center, College Park, Maryland

XUNGANG YIN

Riverside Technology, Inc. (government contractor for NOAA/NCEI), Asheville, North Carolina

HUAI-MIN ZHANG

NOAA/National Centers for Environmental Information, Asheville, North Carolina

(Manuscript received 27 August 2019, in final form 29 February 2020)

ABSTRACT

Previous research has shown that the 1877/78 El Niño resulted in great famine events around the world. However, the strength and statistical significance of this El Niño event have not been fully addressed, largely due to the lack of data. We take a closer look at the data using an ensemble analysis of the Extended Reconstructed Sea Surface Temperature version 5 (ERSSTv5). The ERSSTv5 standard run indicates a strong El Niño event with a peak monthly value of the Niño-3 index of 3.5°C during 1877/78, stronger than those during 1982/83, 1997/98, and 2015/16. However, an analysis of the ERSSTv5 ensemble runs indicates that the strength and significance (uncertainty estimates) depend on the construction of the ensembles. A 1000-member ensemble analysis shows that the ensemble mean Niño-3 index has a much weaker peak of 1.8°C, and its uncertainty is much larger during 1877/78 (2.8°C) than during 1982/83 (0.3°C), 1997/98 (0.2°C), and 2015/16 (0.1°C). Further, the large uncertainty during 1877/78 is associated with selections of a short (1 month) period of raw-data filter and a large (20%) acceptance criterion of empirical orthogonal teleconnection modes in the ERSSTv5 reconstruction. By adjusting these two parameters, the uncertainty during 1877/78 decreases to 0.5°C, while the peak monthly value of the Niño-3 index in the ensemble mean increases to 2.8°C, suggesting a strong and statistically significant 1877/78 El Niño event. The adjustment of those two parameters is validated by masking the modern observations of 1981–2017 to 1861–97. Based on the estimated uncertainties, the differences among the strength of these four major El Niño events are not statistically significant.

1. Introduction

El Niño–Southern Oscillation (ENSO) is one of the dominant modes of Earth's climate system and plays an important role in the reliability of seasonal-to-interannual predictions of temperature and precipitation (Kumar et al. 2000; L'Heureux et al. 2015; Hu et al. 2020). ENSO can significantly impact the life and property over the world, particularly when an ENSO event is strong (Changnon 1999; Goddard and Dilley 2005).

There are different ways to measure the strength or magnitude of historic ENSO events. These factors include which region the sea surface temperature (SST) anomaly (SSTA) is used to quantify the strength of El Niño, how the SSTA is calculated, and which observational datasets (in situ, proxies, etc.) are used. To characterize the ENSO events in the different locations of the equatorial Pacific, SSTA indices were defined in the Niño-3 (5°S–5°N, 90°–150°W), Niño-3.4 (5°S–5°N, 120°–170°W), and Niño-4 (5°S–5°N, 160°E–150°W) regions (Zebiak and Cane 1987).

Another factor affecting the definition of ENSO is how to define the climatology and anomaly. The World

Denotes content that is immediately available upon publication as open access.

Corresponding author: Boyin Huang, boyin.huang@noaa.gov

DOI: 10.1175/JCLI-D-19-0650.1

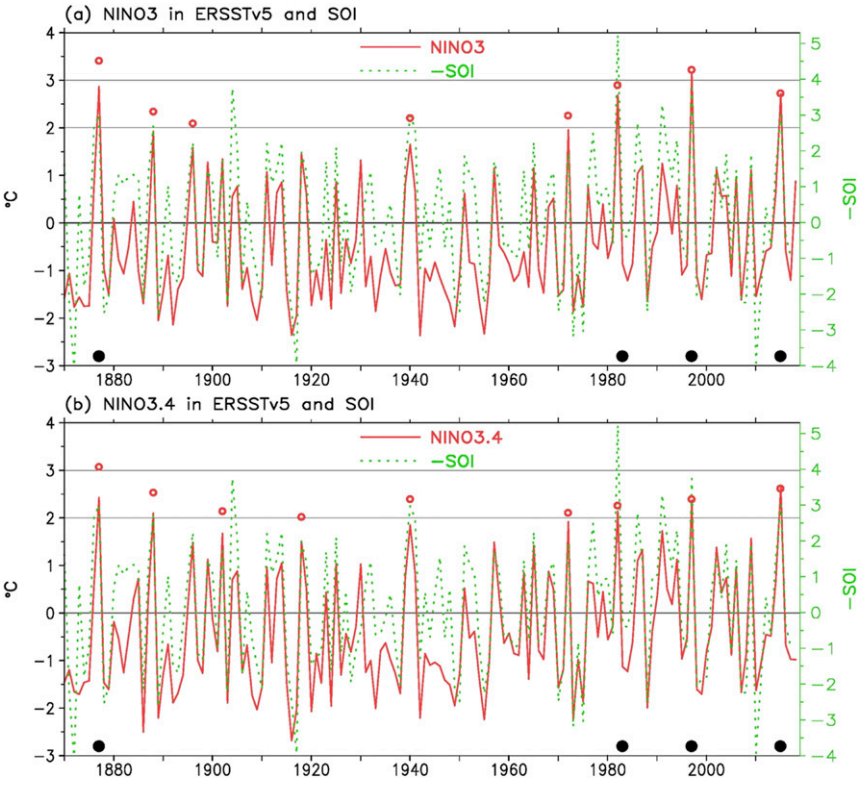

FIG. 1. Average (from October to next March) indices of (a) Niño-3 and (b) Niño-3.4 (solid red line and red circle; left axis) in ERSSTv5 overlapping with −SOI (dotted green; right axis). The red solid lines represent the indices using 1971–2000 climatology, and the red circles represent the indices (>2.0°C) using a 30-yr running average. The time of El Niño events over 1877/78, 1982/83, 1997/98, and 2015/16 is indicated by filled black circles. The correlation coefficient between Niño-3/Niño-3.4 and −SOI is 0.80/0.84, respectively.

Meteorological Organization (WMO) recommends the use of a 30-yr climatology to define anomalies over the historical record. Extending that perspective, the NOAA Climate Prediction Center adopted multiple, overlapping 30-yr base periods to define ENSO events on monthly and seasonal time scales (https://www.cpc.ncep.noaa.gov/products/analysis_monitoring/ensostuff/ONI_v5.php). This change was implemented because observational datasets used to monitor ENSO exhibit long-term warming trends in tropical Pacific SSTA (Latif et al. 1997; Knutson and Manabe 1998; Curtis and Hastenrath 1999; Huang and Liu 2001; Deser et al. 2010; Ashok et al. 2012; L'Heureux et al. 2013).

Studies indicate that the frequency, duration, and strength of ENSO vary from decade to decade (Enfield 1988; Trenberth and Hoar 1996: Rajagopalan and Cook 2000; Yuan et al. 2009; Hu et al. 2013; McGregor et al. 2013; Cai et al. 2014; Latif et al. 2015; Wittenberg 2015; Räsänen et al. 2016; Wang et al. 2017; Capotondi and Sardeshmukh 2017; Li et al. 2019). Recently, there has been debate over whether ENSO events are becoming more frequent and intense (Lee and McPhaden 2010; Newman et al. 2011; Stevenson, 2012; Cai et al. 2014). Some of them have also argued that the number of the central-Pacific (CP) ENSO have increased in the past decades (Larkin and Harrison 2005; Ashok et al. 2007; Newman et al. 2011; Johnson 2013; Yu and Kim 2013). In contrast, others suggest ENSO events in the distant past may be as strong as those observed in recent decades (Enfield 1988; Quinn and Neal 1995; Grove 1998; Räsänen et al. 2016; Singh et al. 2018).

The monthly SSTA relative to a climatology over 1971–2000, for example in the Extended Reconstructed Sea Surface Temperature version 5 (ERSSTv5; Huang et al. 2017), shows that the 1997/98 El Niño in the Niño-3 region was the strongest since the 1870s (Fig. 1a, solid red). However, the monthly SSTA in the Niño-3.4 region (Fig. 1b, solid red) implies that the 2015/16 El Niño event in the central tropical Pacific was the strongest. Niño-3.4 tends to be emphasized by operational ENSO forecasters because this region has stronger correlations with atmospheric variables that comprise ENSO (Barnston et al. 1997), although the leading mode of SSTA variability in the tropical Pacific reveals the

largest loadings in the Niño-3 region (Takahashi et al. 2011).

In contrast, when the impact of warming trend is excluded by subtracting a 30-yr moving climatology, both the Niño-3 and Niño-3.4 indices (Fig. 1, red circles) reveal that the 1877/78 El Niño is among the strongest El Niños in the historical record (Diaz and McCabe 1999; Aceituno et al. 2009; Singh et al. 2018). The existence of the strong 1877/78 El Niño event is supported by independent data sources other than SST, such as the Southern Oscillation index (SOI; Trenberth 1984; Ropelewski and Jones 1987) derived from sea level pressure (Fig. 1, dotted green), the drought indices derived from tree rings and corals, and records of famine or food production around the world (Kiladis and Diaz 1986; Allan et al. 1991; D'Arrigo et al. 2008; Garden 2008; Hao et al. 2010; Räsänen et al. 2016; Singh et al. 2018; Lough et al. 2018). The negative SOI (−SOI) is highly correlated with the Niño-3 (0.80) and Niño-3.4 (0.84) indices.

Therefore, it remains an open question whether the 1877/78 El Niño is truly among the strongest events. The answer may affect our understanding of the relationship between ENSO and a warming climate. If the 1877/78 El Niño is indeed among the strongest, it may suggest that the warming climate has not necessarily enhanced the ENSO amplitude (Enfield 1988; Quinn and Neal 1995; Grove 1998; Räsänen et al. 2016; Singh et al. 2018). However, this does not exclude the idea that these stronger events have become more frequent in the recent record (Lee and McPhaden 2010; Newman et al. 2011; Stevenson 2012; Cai et al. 2014).

The difficulty in quantifying the strength of the 1877/78 El Niño is that there are limited in situ SST observations (Fig. 2a), and therefore an ensemble analysis from ERSSTv5 is used in this study. In addition, regardless of the ultimate characterization in the strength of the 1877/78 El Niño, it is important to document dataset availability and reliability, which was not analyzed closely in the aforementioned studies. Generally, observations over the global oceans are sparser and less reliable in the past compared with modern times (Freeman et al. 2017). For example, the areal coverage of in situ SST observations in 2° × 2° grid boxes is lower in the 1900s and 1950s (30%–40%) than in the 2000s (70%) (Huang et al. 2017). Consequentially, biases and random errors of SST observations are larger before the 1950s than after (Kennedy et al. 2011a,b; Huang et al. 2016b, 2020).

To determine whether one El Niño event is stronger than the other, we need to quantify not only their magnitude, but also their uncertainty, and to test whether the difference between these events is statistically significant (e.g., Huang et al. 2016a), as is done here. In this paper, ERSSTv5 and its uncertainty quantification are briefly described in section 2. In section 3, the magnitude and uncertainty of the 1877/78 El Niño event are compared to the 1997/98 El Niño event since the maximum SSTAs were located in the east-central tropical Pacific during both events. The dominant factors contributing to the uncertainty of these two El Niño events are analyzed in sections 4a–4c. The capability of ERSSTv5 in representing the strength and uncertainty of the 1877/78 El Niño is verified in sections 4d and 4e. Results are summarized in section 5.

2. ERSSTv5 and its uncertainty

ERSSTv5 is a monthly 2° × 2°SST product from 1854 to the present and reconstructs SSTs from in situ ships, buoys, and Argo floats (Huang et al. 2017). Ship and buoy observations are from the International Comprehensive Ocean–Atmosphere Dataset (ICOADS) R3 (Freeman et al. 2017). Temperature observations from Argo floats are downloaded from the Global Data Assembly Centre (GDAC; https://www.seanoe.org/data/00311/42182/), and near-surface temperatures of 0–5-m depth are defined as SSTs. The biases of ship SSTs are corrected with reference to nighttime marine air temperature (NMAT) from the U.K. Hadley Centre (HadNMAT2; Kent et al. 2013) before 1985 and with reference to buoy SSTs after 1985. The Argo SSTs are close to buoy SSTs (less than 0.03°C overall) and are corrected with reference to buoy SSTs. The homogenized ship and Argo SSTs represent buoy SSTs at a nominal depth of 0.2 m. The bias-corrected SSTs over the global oceans are then fitted to a maximum of 140 leading empirical orthogonal teleconnection functions (EOTs; van den Dool et al. 2000; Smith and Reynolds 2004). It was found that spatial and temporal variabilities of SSTs in ERSSTv5 are more realistic and more reliable than those in previous versions of ERSST (v4 and v3b) over the global oceans (Huang et al. 2017, 2019).

Nevertheless, the ERSSTv5 analysis, like other similar types of analyses, exhibits uncertainties. The uncertainties generally result from incomplete data sampling in space and time and from observation errors. For SST analysis, there are two types of observation errors: One is associated with occasional human mistakes in reading thermometers, and the other is associated with systematic biases due to changes in thermometer types and measurement protocols. Many algorithms have been developed to minimize the impact of these errors in SST analyses using quality control procedures, bias adjustments, gridding, interpolation, and analysis methodologies (Smith and Reynolds 2003, 2004; Kennedy et al. 2011a,b; Huang et al. 2016a,b). In ERSSTv5 and

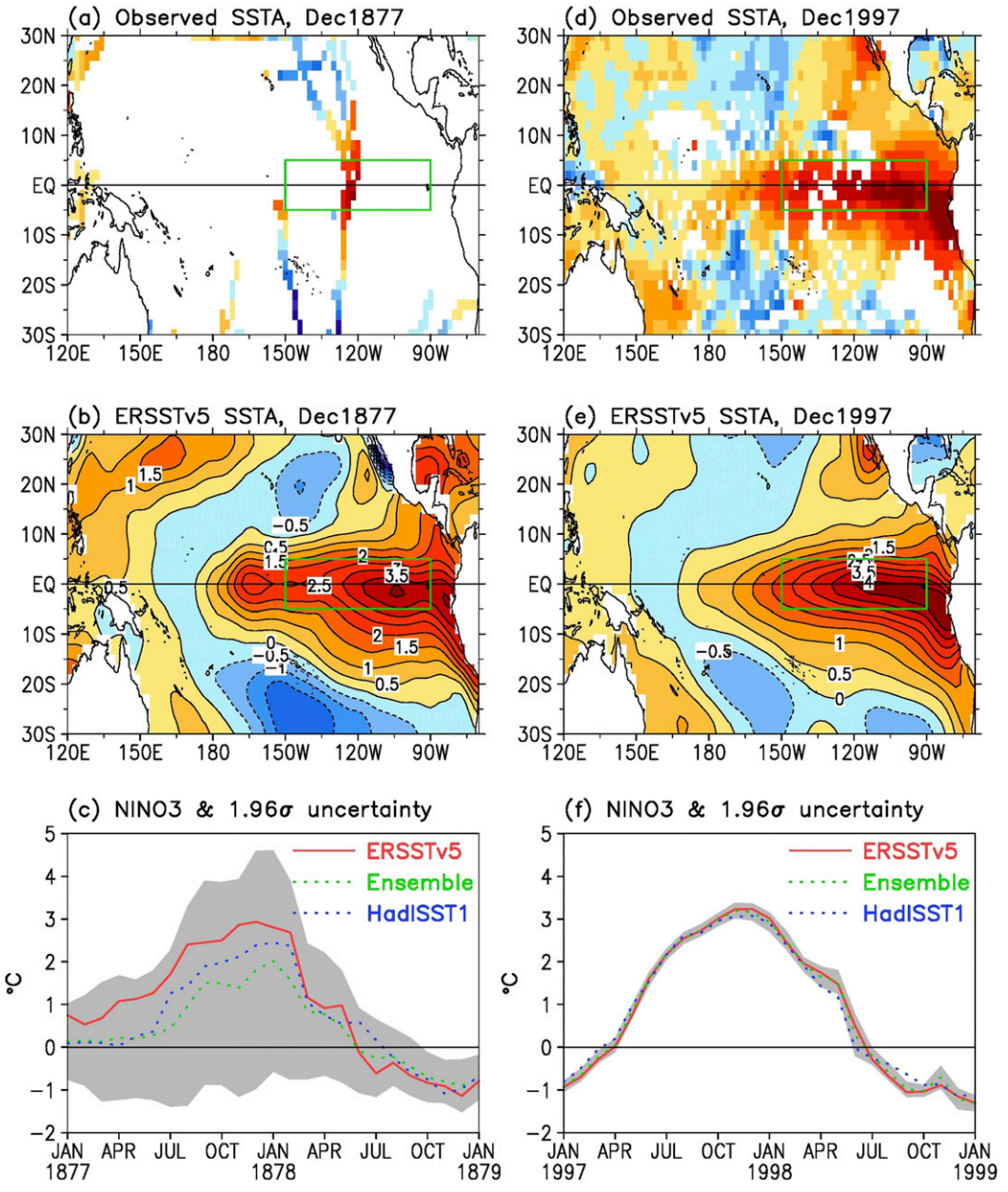

FIG. 2. (a) Observed SSTA and (b) ERSSTv5 SSTA in December 1877, and (c) Niño-3 in ERSSTv5 (solid red), EN = 1000 ensemble average (dotted green) and its 1.96σ uncertainty between January 1877 and January 1879. (d),(e) As in (a),(b), but for December 1997; (f) as in (c), but between January 1997 and January 1999. The Niño-3 index (dotted blue) from the Hadley Centre Sea Ice and Sea Surface Temperature dataset (HadISST1; Rayner et al. 2003) is overlapped for intercomparison purpose. Color scales in (a), (b), (d), and (e) are the same.

ERSSTv4, the total uncertainty (U_t) of SST consists of reconstruction (U_r) and parametric (U_p) uncertainties (Huang et al. 2016a,b, 2020):

$$U_t^2 = U_p^2 + U_r^2. \quad (1)$$

The reconstruction uncertainty is associated with using a limited set of EOTs, and is generally constant in time and small (less than 0.1°C) for regional averaged SST such as Niño indices. The parametric uncertainty is associated with the changes in selecting parameters in ERSSTv5 reconstruction. The reconstruction uncertainty is generally much smaller than the parametric uncertainty for a regional averaged SST. Here we simply use ''uncertainty'' to represent the total uncertainty quantified in Eq. (1).

There are 28 independent parameters in ERSSTv5 reconstruction (Huang et al. 2016b, 2020) that control reconstruction factors related to the quality control (QC) of observations, bias correction of ship SSTs, the selection of 140 leading EOTs, and others (Huang et al. 2017). For the ERSSTv5 uncertainty estimates studied here, each of the 28 parameters can have 2–7 alternative options. By randomly selecting these options with equal probability for the 28 parameters, a 1000-member ensemble is produced. The parametric uncertainty of ERSSTv5 is estimated based on the 1000-member ensemble SSTAs relative to the 1971–2000 climatology. In this study, we find that the following two parameters can critically influence the El Niño estimates.

a. High-frequency 3-month filter

The lag-1 autocorrelation of monthly SSTs is large (approximately 0.77 in the global ocean and 0.88 in the tropical Pacific) as expected due to the slow variation of ocean temperature associated with the high heat content of water. Therefore, a high-frequency (HF) filter of 3 months is applied when SST superobservations (superobs hereafter) are not valid, and the invalid superobs are replaced using superobs at the previous and next months. The superobs are bin averages of raw SST observations within 2° × 2° grid boxes. Two options are selected to produce the 1000-member ensemble: HF = 3mon (with HF filter) and HF = 1mon (without HF filter) and represent the contribution of HF to the uncertainty in ERSSTv5 in Eq. (1). The selection of HF = 3mon increases the areal coverage of superobs in ERSSTv5, while the selection of HF = 1mon uses actual in situ observations at current month and therefore reduces the areal coverage.

b. EOT acceptance criterion

In the ERSSTv5 reconstruction, not all 140 EOT modes are used each month. An EOT mode $[E_i(x)]$ was accepted only if its variance ratio (r_i) is greater than an acceptance criterion (Crit):

$$r_i = \frac{\left[\sum_x E_i^2(x)\delta_x \cos\varphi_x\right]}{\left[\sum_x E_i^2(x)\cos\varphi_x\right]} > \text{Crit}, \qquad (2)$$

where δ_x is set to 0 or 1 dependent on whether the superobs have a valid datum at a 2° × 2° grid box x, and φ_x represents latitude. Three criteria of 5%, 10%, and 20% are artificially selected in generating the 1000-member ensemble to represent the contribution of Crit to the parametric uncertainty. The parameter Crit measures whether a particular EOT mode is supported by superobs or not (i.e., may potentially be an artifact without sufficient observational support). The higher the Crit, the more superobs are required within the area of an EOT mode to accept this EOT mode in the reconstruction. The selections of Crit = 20% and 10% were based on previous versions of ERSST (v3b andv4). Crit = 5% is set as a lower limit to evaluate the potential impact of Crit in estimating the parametric uncertainty of ERSSTv5. In the operational ERSSTv5 dataset Crit was set to 10% (Huang et al. 2017).

3. Comparing the 1877/78 El Niño with other El Niño events

a. The 1877/78 El Niño and its uncertainty

Previous studies have corroborated the strong El Niño during 1877/78 using various datasets (Kiladis and Diaz 1986; Diaz and McCabe 1999; Aceituno et al. 2009; Quinn and Neal 1995; Grove 1998; Hao et al. 2010; Huang et al. 2015). However, there were few in situ SST observations at that time. As an example, Fig. 2a shows the observational coverage over the tropical Pacific (30°S–30°N, 120°E–70°W) in December 1877. These sparse SST records in the east-central Pacific (Fig. 2a) were measured during 14–31 December 1877 and provided by Deutsche Seewarte Marine (ship ID 120) and Met Office Marine Data Bank (ship IDs 4238 and 4270). Despite a low areal coverage of SST superobs (approximately 7%), the ERSSTv5 standard/operational run shows a strong El Niño with a peak magnitude of 4.0°C in the east-central tropical Pacific (Fig. 2b). The Niño-3 index also reaches its maximum (2.9°C; Table 1) in December 1877 (Fig. 2c, solid red), consistent with the large negative SOI (Fig. 1a).

In the ERSSTv5 standard/operational run, the parameters HF and Crit are set to 3mon and 10%, respectively, to best represent ENSO events in the tropical Pacific (Huang et al. 2017). Other parameter options of HF = 1mon and Crit = 5% or 20% are used in generating the 1000-member ERSSTv5 ensemble to represent the parametric uncertainty of ERSSTv5 when these parameters are perturbed within a reasonable range of 50%–100% (Huang et al. 2020).

After including all these alternative parameter selections in the 1000-member ensemble, the ensemble mean Niño-3 is calculated (Fig. 2c, dotted green), which is approximately 1.1°C lower than the ERSSTv5 standard run values between April 1877 and February 1878 (Fig. 2c, solid red). The ensemble mean Niño-3 is only 1.8°C in December 1877. The reduced Niño-3 index values are accompanied by large spread among the ensemble members. This spread is used to estimate the

TABLE 1. Niño indices and their uncertainties (1.96σ in unit °C) in ERSSTv5, EN = 1000, EN = 482, EN = 652, and EN = 318 in the 1877/78, 1982/83, 1997/98, and 2015/16 events. Indices in parentheses are those after adjustment of 30-yr running average as shown in Fig. 1.

Event	1877/78	1877/78	1982/83	1997/98	2015/16
Index	Niño-3	Niño-3.4	Niño-3	Niño-3	Niño-3.4
ERSSTv5	2.93 (3.47)	2.50 (3.15)	2.92	3.23	2.76
Peak time	Dec 1877	Feb 1878	Jan 1983	Dec 1997	Nov 2015
EN = 1000	1.81 ± 2.78	1.10 ± 1.97	2.75 ± 0.37	3.16 ± 0.20	2.79 ± 0.16
EN = 482	2.60 ± 1.67	1.81 ± 1.45	2.72 ± 0.34	3.15 ± 0.20	2.74 ± 0.13
EN = 652	2.37 ± 1.71	1.52 ± 1.28	2.76 ± 0.37	3.16 ± 0.20	2.80 ± 0.16
EN = 318	2.81 ± 0.54	2.11 ± 0.56	2.72 ± 0.33	3.16 ± 0.20	2.75 ± 0.13

parametric uncertainty in Eq. (1) and the uncertainty at 95% confidence level in ERSSTv5 (Fig. 2c, gray shading). The uncertainty is based on the 95% confidence range (defined by $\pm 1.96\sigma$). Figure 2c shows that the range of Niño-3 uncertainty increases from about 0.9°C in January 1877 to about 2.8°C in December 1877, and decreases to about 0.6°C in January 1879. The large uncertainty, especially in December 1877, indicates that ensemble mean Niño-3 value (1.8°C in December 1877) is not statistically different from zero and is therefore not statistically significant. Further investigation suggests that the Niño-3 uncertainty in the ERSSTv5 ensemble is overestimated in the 1000-member ensemble, and its details will be explored in sections 4a–4c.

b. *Comparison with the 1997/98, 1982/83, and 2015/16 El Niño events*

For a given set of parameter selections of the high-frequency filter (HF) and EOT acceptance criterion (Crit) in the 1000-member ensemble, the SST uncertainty in the Niño regions (e.g., Niño-3; Fig. 3, dotted black) critically depends on the areal coverage of SST superobs in the tropical Pacific (e.g., 30°S–30°N; Fig. 3, dotted green). The uncertainty of Niño-3 is as high as 2.8°C before the 1880s when superobs coverage is lower than 10%, is approximately 1.5°C during the two world wars when superobs coverage is as low as 20%, and decreases to as low as 0.2°C after the 1960s when superobs coverage nears its maximum around 80%. These uncertainties are mostly attributed to the parametric uncertainty, with less than 0.1°C attributed to the reconstruction uncertainty.

The 1997/98 El Niño is a suitable candidate for comparison with the 1877/78 El Niño, because both have a similar maximum SSTA of 4.0°C in the east-central tropical Pacific (Figs. 2b,e) in the ERSSTv5 standard run. The Niño-3 index values in both events are larger than 3.2°C (Table 1). The major difference between these two events, from an SST reconstruction analysis point of view, is that the superobs coverage is much lower during 1877/78 (7%; Figs. 2a and 3) than during 1997/98 (78%; Figs. 2d and 3). This difference results in two features. First, the Niño-3 uncertainty range based on the 1000-member ensemble is reduced from 2.8°C during 1877/78 to 0.2°C during 1997/98 (Table 1). Second, the ensemble mean Niño-3 index matches the

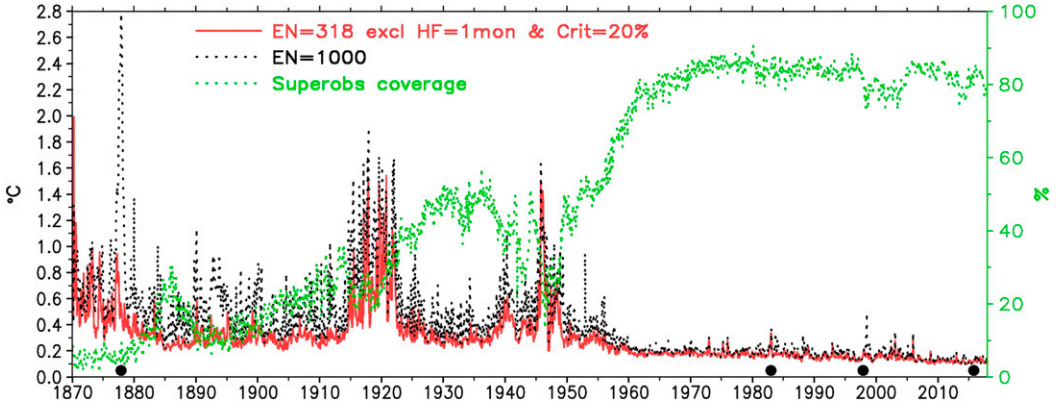

FIG. 3. Monthly uncertainty (1.96σ) of Niño-3 in EN = 1000 (dotted black; left axis) and EN = 318 *excluding* (excl) members of parameters HF = 1mon and Crit = 20% (solid red; left axis). Superobs coverage in the tropical Pacific (30°S–30°N; dotted green; right axis) is overlapped. The time of El Niño events over 1877/78, 1982/83, 1997/98, and 2015/16 is indicated by filled black circles.

ERSSTv5 standard run value during 1997/98 (Fig. 2f), whereas a large difference (1.0°C) arises during 1877/78 (Fig. 2c) between the ERSSTv5 1000-ensemble mean and ERSSTv5 standard run values.

These features can also be seen when the 1982/83 and 2015/16 El Niños are compared (Table 1). During 1982/83, the El Niño maximized in the eastern tropical Pacific, similar to the 1997/98 El Niño, and so its strength is well captured by the Niño-3 index (2.9°C) in ERSSTv5 (Table 1). In contrast to the 1982/83 and 1997/98 events, the maximum SSTA during the 2015/16 event was in the east-central tropical Pacific, which is a mixture of CP and eastern Pacific (EP) types of ENSO (Larkin and Harrison 2005; Ashok et al. 2007) with maximum SSTA in the Niño-3.4 region (2.8°C; Table 1). Due to the high coverage of observations in the modern era (Fig. 3, dotted green), the uncertainty of Niño-3 and Niño-3.4 based on the 1000-member ensemble is small in all three recent events (0.1°–0.3°C; Table 1). A remaining question is whether the strength of the 1877/78 El Niño is distinct from those three strong El Niño events in the modern period (1982/83, 1997/98, and 2015/16), which will be addressed in section 4.

4. Impacts of the parameters Crit and HF on 1877/78 El Niño

a. Factor analysis

As shown in section 3a, the ensemble mean Niño-3 index may have been underestimated and the Niño-3 uncertainty may have been overestimated for the 1877/78 El Niño in the 1000-member ensemble. Which parameters lead to the small Niño-3 index value and the large Niño-3 uncertainty? The question is usually addressed by a method called factor analysis (Huang et al. 2016b), which quantifies the impact of parameters (the 28 parameters in this study) on the variable of interest (here, the Niño-3 index in December 1877):

(i) 1000 members of the Niño-3 index are calculated for December 1877 and paired with the randomly selected options of the 28 parameters.
(ii) The Niño-3 index values in December 1877 are grouped into different subensembles by *excluding* certain selections (e.g., HF = 1mon or HF = 3mon) out of the 28 parameters. The number of subensembles per parameter is equal to the number of that parameter's options [for a maximum of 7; Table 2 in Huang et al. (2020)].
(iii) The ensemble-averaged Niño-3 and its standard deviation (STD) within subensembles are calculated, and their differences relative to those within the 1000-member ensemble are evaluated by that particular parameter. The STD is used to quantify the sensitivity of Niño-3 to the changes in ERSSTv5 parameters.
(iv) The factor analysis of (i)–(iii) is repeated for all 28 parameters to determine which particular parameters contribute to a small Niño-3 index value and large Niño-3 uncertainty in December 1877.

Figure 4a shows that parameter 22 (HF) and 25 (Crit) are the two dominant parameters whose particular selection of their alternative options within the 1000-member ensemble can greatly impact the Niño-3 index value in December 1877. When HF selection of 1 or 3 months is excluded, the Niño-3 index increases or decreases by approximately 0.8°C. When Crit = 20% or Crit = 5% is excluded, the Niño-3 index increases or decreases by 0.6°C. In contrast, the impacts from the other 26 parameters are small (<0.2°C). The subensembles (Fig. 4b) also reduce Niño-3 STD by approximately 1.1°C when HF = 1mon or Crit = 20% is excluded, whereas little impact is found from other 26 parameters or other selections of HF and Crit. These results suggest that the selection of HF = 1mon and Crit = 20% could be responsible for the characteristics of the Niño-3 index in the 1000-member ensemble.

In contrast to the influence of HF = 1mon and Crit = 20% on the 1877/78 El Niño, their impacts on the Niño-3 index (Fig. 4c) and Niño-3 STD (not shown) during the 1997/98 El Niño are very small. The contrast is largely associated with the difference in SST superobs coverages between these two events. When SST superobs coverage is large (80%), as in the 1997/98 El Niño, ERSSTv5 is not sensitive to the selections of the 28 parameter values.

Even when the Niño-3.4 or Niño-4 index is analyzed or a different month (e.g., November 1877 or January 1878) is chosen, the preceding results do not vary significantly.

b. SSTA and its uncertainty in subensembles

The factor analysis in section 4a shows that the Niño-3 index and its uncertainty in December 1877 are clearly impacted by selections of HF and Crit in the 1000-member ensemble. To further demonstrate how the selections of HF and Crit impact the Niño-3 index and its uncertainty during the 1877/78 El Niño, the 1000-member ensemble is grouped into four subensembles as in section 4a, which are labeled with different number of subensemble members (EN): (i) EN = 1000 by including all ensemble members, (ii) EN = 482 by excluding members of HF = 1mon, (iii) EN = 652 by excluding members of Crit = 20%, and (iv) EN = 318 by excluding members of both HF = 1mon

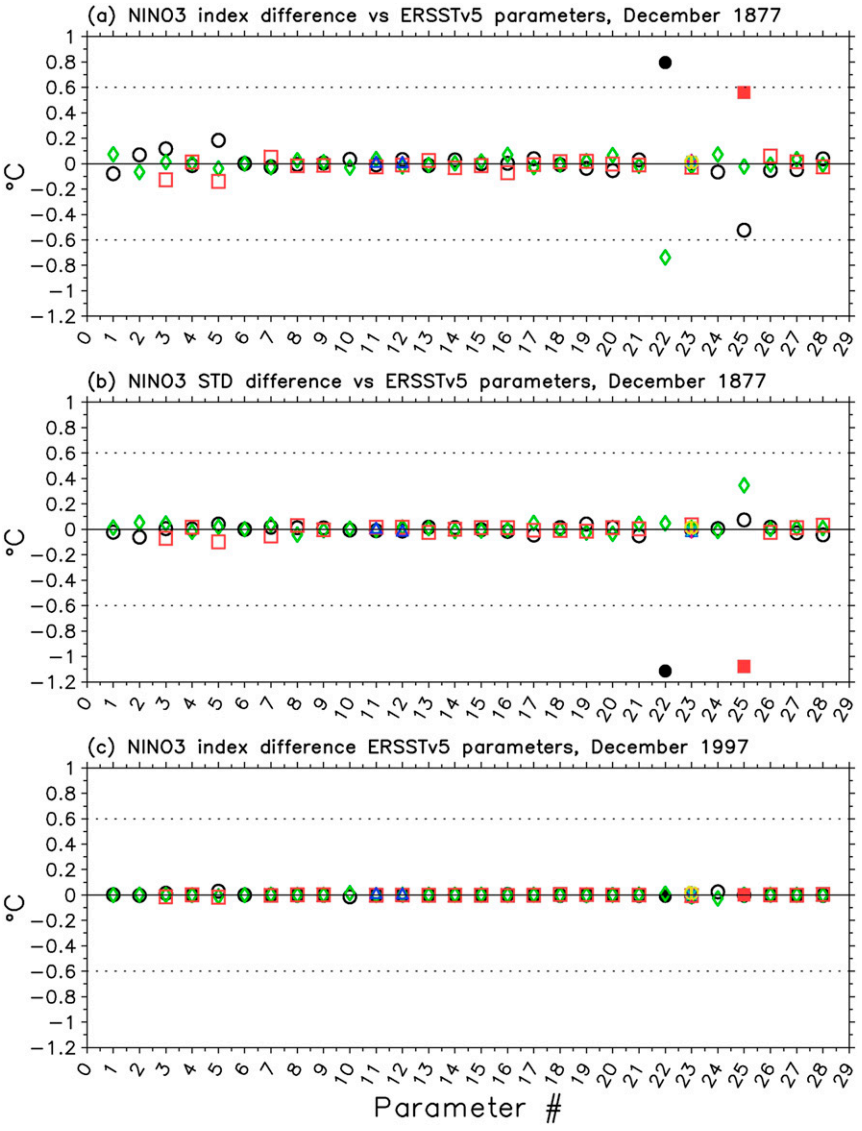

FIG. 4. Factor analyses of (a) differences of the Niño-3 index in December 1877, (b) differences of the Niño-3 STD in December 1877, and (c) differences of the Niño-3 index in December 1997. Differences are calculated between subensembles and 1000-member ensemble. Subensembles are calculated by excluding one option (maximum 7) of a particular parameter, and represented by black circle, green diamond, red square, blue triangle, light-blue cross, magenta plus sign, and yellow open cycle with vertical bar, respectively. The x axis represents one of 28 parameters (Table 2; Huang et al. 2019). The circle and square are highlighted by filling in parameter-22 (HF = 1mon) and parameter-25 (Crit = 20%).

and Crit = 20%. These EN numbers in (ii)–(iv) are calculated based on randomly selected HF and Crit values out of the 1000 ensemble members.

Using these four subensembles, the Niño-3 index and its uncertainty within each subensemble are calculated (Fig. 5). Figure 5 shows two features after excluding unrealistic members: First, the ensemble mean Niño-3 index values during January 1877 and March 1878 increases from EN = 1000 to EN = 482, EN = 652, and EN = 318 (Figs. 5a–d, dotted green). The Niño-3 index values in EN = 318 (Fig. 5d, dotted green) are close to the ERSSTv5 standard run values (Fig. 5d, solid red). SSTAs clearly strengthen in the Niño-3.4 region (Table 1) and across the tropical Pacific (Figs. 6a–d). For example, the Niño-3 index value in December 1877 is 1.8°, 2.6°, 2.4°, and 2.8°C (Table 1); maximum SSTA is 2.0°, 3.5°, 3.0°, and 3.5°C (Figs. 6a–d); and the 2°C contour extends westward at 120°, 150°, 140°, and

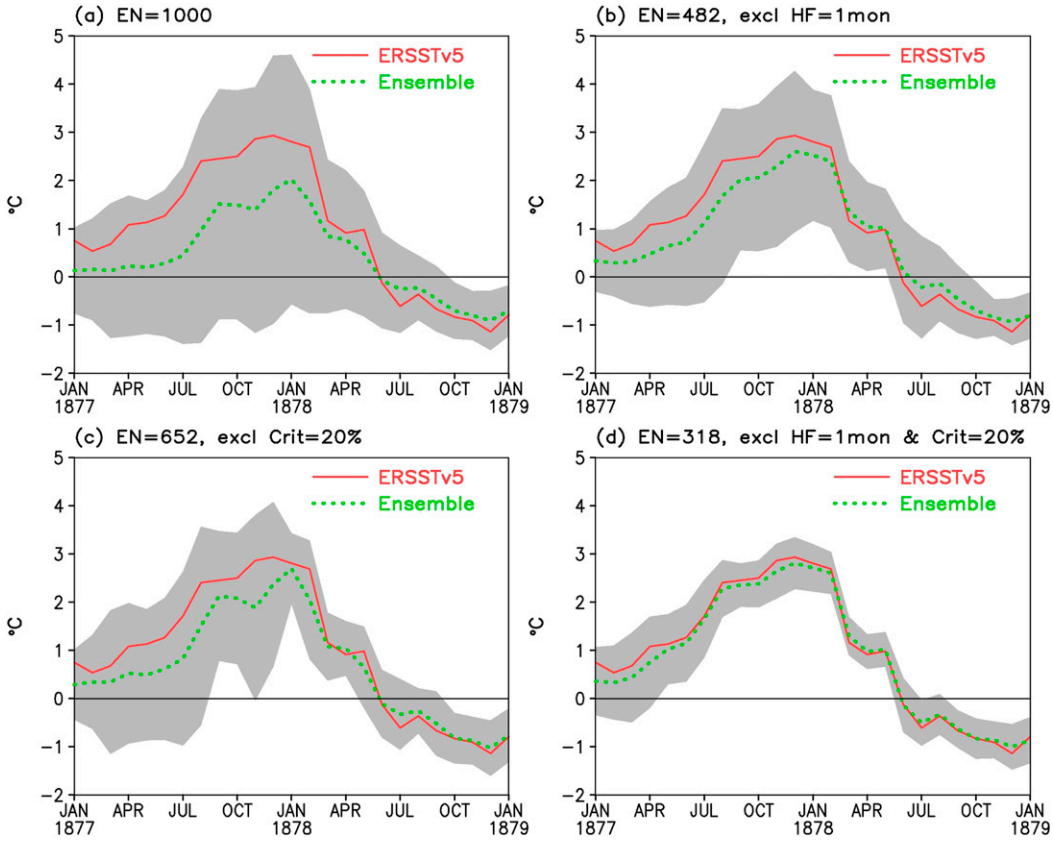

FIG. 5. Niño-3 index in ERSSTv5 (solid red) and its 1.96σ uncertainty (gray shading) centered with ensemble average (dotted green) in (a) EN = 1000, (b) EN = 482 excluding (excl) members of HF = 1mon, (c) EN = 652 excluding members of Crit = 20%, and (d) EN = 318 excluding members of HF = 1mon and Crit = 20%.

160°W in the subensembles EN = 1000, EN = 482, EN = 652, and EN = 318, respectively, although overall spatial patterns of SSTAs over the tropical Pacific are similar.

Second, the Niño-3 uncertainty (Figs. 5a–d, gray shading) decreases dramatically from EN = 1000, EN = 652, EN = 482, to EN = 318, particularly from January 1877 to March 1878. The uncertainty values in December 1877 are approximately 2.8°, 1.7°, 1.7°, and 0.5°C, respectively (Table 1). The reduction of SST uncertainty is similar in the Niño-3.4 region (Table 1) and across the east-central tropical Pacific. For example, Fig. 7 shows that the SST STD among the ensemble members in the east-central tropical Pacific is as high as 3°C when all 1000 members are included (EN = 1000; Fig. 7a). The STD reduces to 2°C when members of HF = 1mon (EN = 482) or Crit = 20% (EN = 652) are excluded (Figs. 7b,c), and further reduces to less than 1°C (EN = 318; Fig. 7d) when members of both HF = 1mon and Crit = 20% are excluded.

In contrast, the Niño-3 and Niño-3.4 indices and their uncertainties during the 1997/98 and 2015/16 El Niño are not sensitive to those two parameters of HF and Crit, and their uncertainties are much smaller, around 0.1°–0.2°C (Table 1). These comparisons confirm that selections of HF and Crit values can only make a difference when observations are sparse. The negative correlation (approximately −0.68) between the SST uncertainty and observational coverage is significant not only during ENSO events, but also during ENSO-neutral years (Fig. 3, dotted black and dotted green). When selections of both HF = 1mon and Crit = 20% are excluded, uncertainties of Niño-3 (Fig. 3, solid red) and Niño-3.4 (not shown) decrease during the 1870s to 1950s, and the reduction becomes smaller after the 1960s when the observational coverage is high (>70%; Fig. 3, dotted green).

It should be noted that the different size of ensemble members used here does not affect the statistical features discussed in sections 4a and 4b because the smallest size of members (EN = 318) is still large enough (Huang et al. 2016b). Tests show that the Niño indices and their uncertainty remain similar when the size of ensemble members is reduced to 318. However, it is not completely clear why selections of HF = 1mon and Crit = 20% result in smaller SSTA and large SST

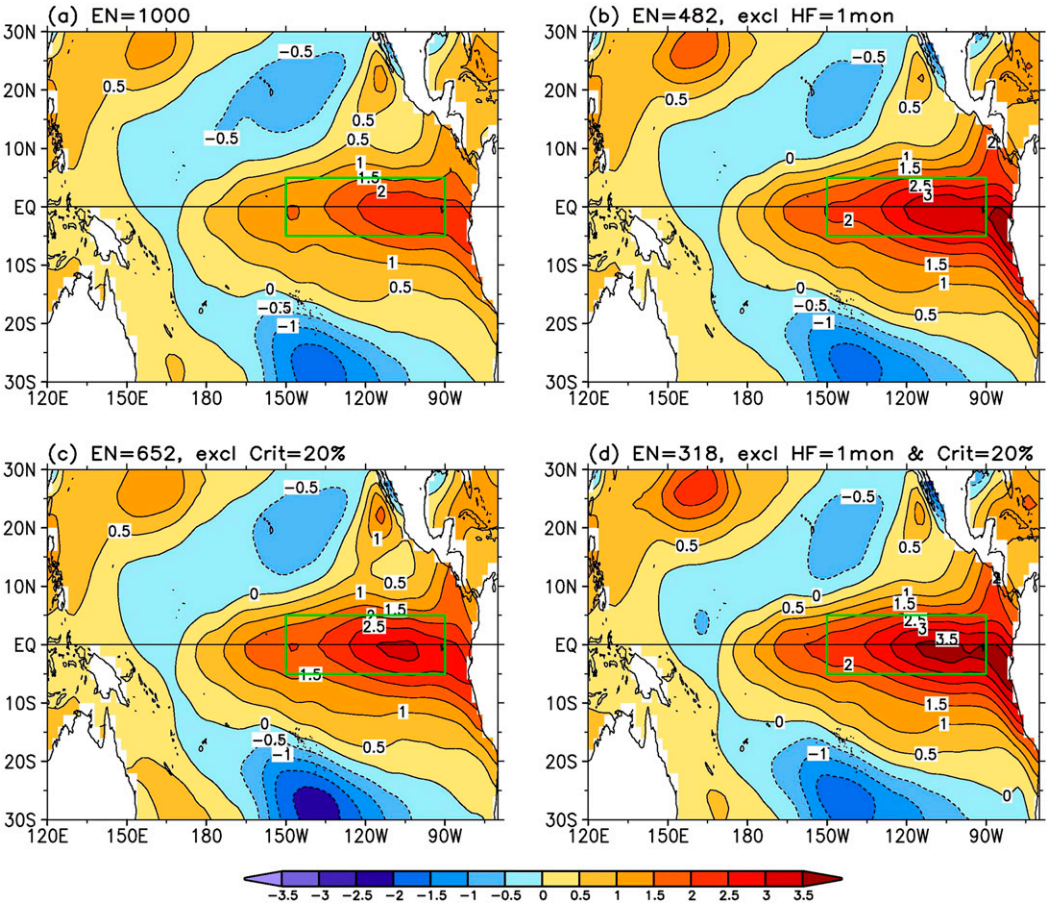

FIG. 6. Ensemble averaged SSTA in December 1877 in (a) EN = 1000, (b) EN = 482 excluding (excl) members of HF = 1mon, (c) EN = 652 excluding members of Crit = 20%, and (d) EN = 318 excluding members of HF = 1mon and Crit = 20%.

uncertainties across the tropical Pacific, which is explored further in the next section.

c. *Reasons for small Niño index values*

To further understand the consequences of selecting HF = 1mon and Crit = 20%, four experiments (EXs) are designed in parallel with ERSSTv5 by resetting HF and Crit while other 26 parameters (Table 2 in Huang et al. 2020) remain unchanged: EX-1: HF = 3mon and Crit = 10% as in the standard/operational ERSSTv5, EX-2: HF = 1mon and Crit = 10%, EX-3: HF = 3mon and Crit = 20%, and EX-4: HF = 1mon and Crit = 20%. Figures 8a–d show SSTAs in January 1878 when parameters of HF and Crit are set in EXs 1–4, respectively. January 1878 is the focus because this month is less complicated and projects mostly onto fewer, lower-order EOTs 1, 2, 3, and 6, while other winter months also project onto several higher-order EOTs.

These experiments show that ERSSTv5 is able to successfully capture the 1877/78 El Niño with a similar spatial pattern in EXs 1–3 (Figs. 8a–c). The spatial correlation is 0.91 between EX-1 and EX-2 and 0.87 between EX-1 and EX-3, although the maximum SSTA is slightly weaker in EX-2 and EX-3 (3.0°C) than in EX-1 (3.5°C). However, EX-4 (Fig. 8d) fails to represent the El Niño event with reduced SSTAs in the tropical Pacific. To investigate the reason for the success and failure in representing the El Niño event, EOT variances ratios (Table 2) are calculated for EOTs 1, 2, 3, and 6 in the tropical Pacific (Fig. 9, contours). Note that EOTs 4 and 5 are outside the tropical Pacific. By comparing EOT variance ratio r_i with EOT acceptance criterion (Crit), we can elucidate which EOTs are accepted in SSTA reconstruction and how the acceptance of EOTs impacts the overall SST reconstruction.

As shown in Eq. (2), EOT variance ratios and therefore EOT acceptance depend on the superobs coverage associated with δ_x, which relies on the selection of HF. When HF = 3mon is selected, superobs coverage is relatively high (Fig. 9, gray + yellow shading), variance ratios of EOT-1, EOT-3, and EOT-6 are above 20% (Table 2).

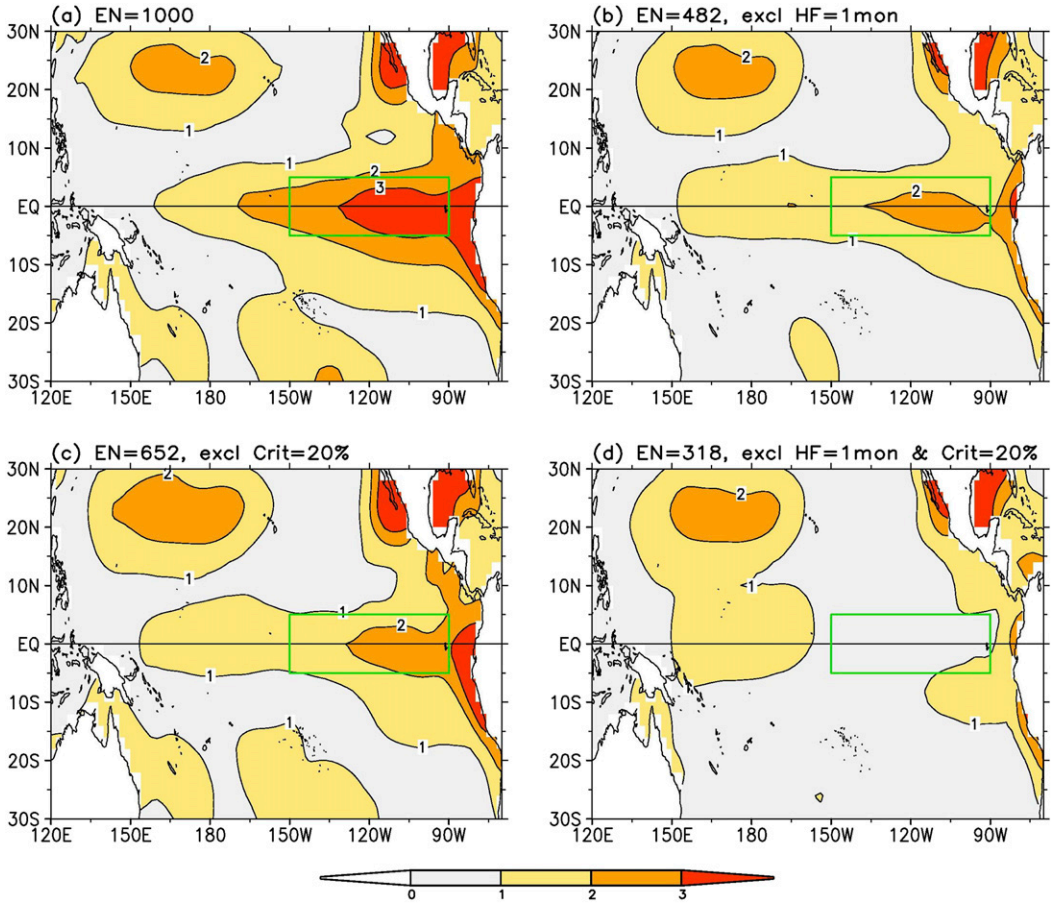

FIG. 7. SST STD (1σ) in December 1877 in ensemble (a) EN = 1000, (b) EN = 482 excluding (excl) members of HF = 1mon, (c) EN = 652 excluding members of Crit = 20%, and (d) EN = 318 excluding members of HF = 1mon and Crit = 20%.

Therefore, these three EOTs are accepted whether Crit is set to 10% or 20%. In contrast, when HF = 1mon is selected, superobs coverage is low (Fig. 9, yellow shading), only the variance ratio of EOT-6 is above 20% while variance ratios of EOT-1 and EOT-3 are between 10% and 20% (Table 2). Therefore, EOT-1, EOT-3, and EOT-6 are accepted when Crit is set to 10%, but only EOT-6 is accepted when Crit is set to 20%. As a result, when HF = 1mon and Crit = 20% are set in EX-4 (Fig. 8d), EOT-1 and EOT-3 are rejected, and SSTA reconstruction fails since these two modes are critical to represent El Niño events. In contrast, EOT-1 and EOT-3 are accepted in EX 1–3 so that the 1877/78 El Niño is well represented (Figs. 8a–c). Note that EOT-2 is rejected in all experiments, since there were almost no data in its loading center area (western Pacific) in January 1878.

d. Verification

Analyses in sections 4b and 4c suggest that the combined parameter options of HF = 1mon and Crit = 20% should be excluded in order to reasonably represent the magnitude and uncertainty of the 1877/78 El Niño in the ERSSTv5 ensemble runs. As such, how can we ensure that various HF and Crit options are properly representing the pattern and strength of the 1877/78 El Niño in ERSSTv5? To analyze this, an SST reconstruction over the 1861–97 period is simulated using the superobs over 1981–2017 in the following two steps:

1) The superobs in the modern observation-rich period of 1981–2017 are reduced using the superobs masks from 1861–97. Therefore areal coverages of reduced superobs during 1981–2017 become identical to those during 1861–97.
2) The reduced superobs during 1981–2017 are then reconstructed. If this reconstructed ERSSTv5 is able to properly represent the 1997/98 El Niño, we can conclude that the representation of 1877/78 El Niño in ERSSTv5 is also a valid reconstruction because the 1997/98 El Niño is well observed by modern technology.

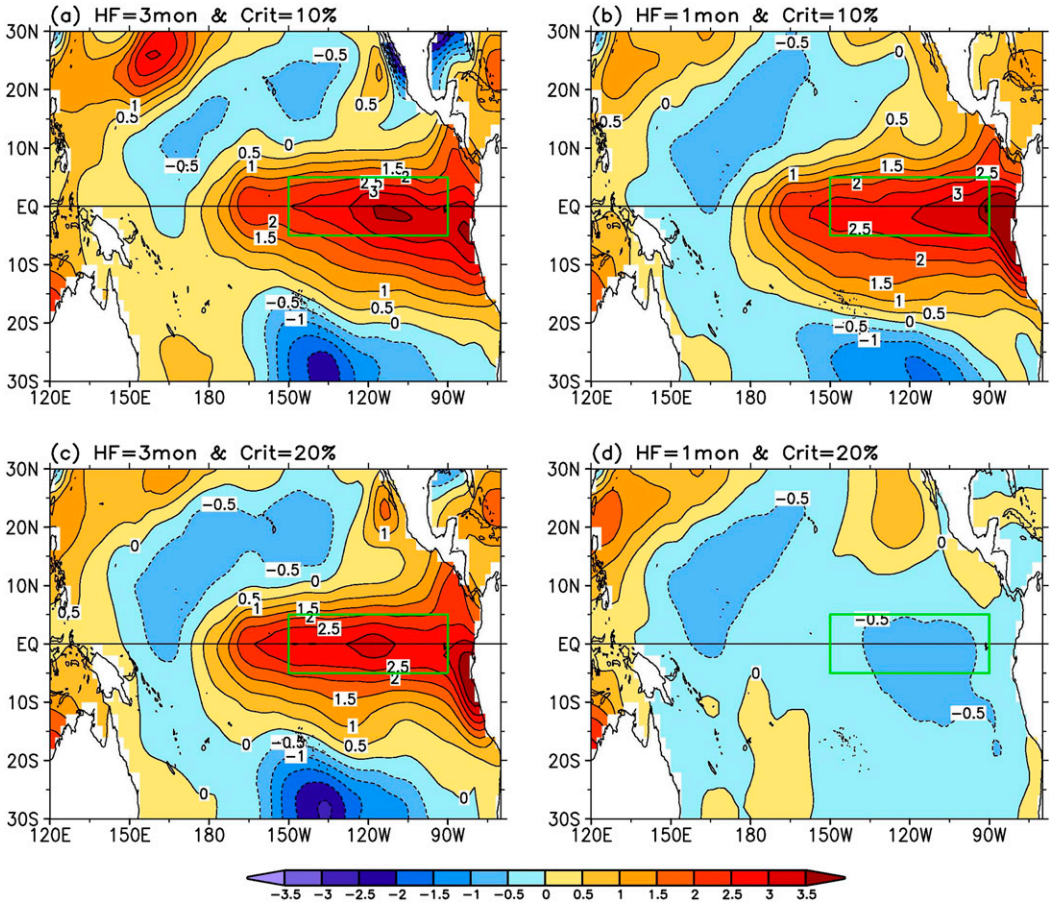

FIG. 8. SSTAs in January 1878 in ERSSTv5 experiments using (a) HF = 3mon and Crit = 10%, (b) HF = 1mon and Crit = 10%, (c) HF = 3mon and Crit = 20%, and (d) HF = 1mon and Crit = 20%.

By applying the above procedure, four ERSSTv5 experiments similar to those in section 4c are designed using different selections of parameter values for HF and Crit (EX-1: HF = 3mon and Crit = 10%; EX-2: HF = 1mon and Crit = 10%; EX-3: HF = 3mon and Crit = 20%; and EX-4: HF = 1mon and Crit = 20%) while the other 26 parameters are kept unchanged. The success or failure in representing the 1997/98 El Niño in those four experiments is an indicator of the capability of ERSSTv5 in representing the 1877/78 El Niño.

Figure 10a shows the ERSSTv5 SSTA for January 1998, with a maximum SSTA of 3.5°C in the east-central tropical Pacific. The spatial distribution and magnitude of this El Niño are well represented in EXs 1–3 (Figs. 10b–d). Their similarity is quantified by a high spatial correlation coefficient (0.92–0.96) between ERSSTv5 and EXs 1–3. The evolution of Niño-3 indices (Fig. 11) is also highly consistent between ERSSTv5 (solid black) and EXs 1–3 (solid red, dotted green, and dotted blue). Temporal correlation coefficients between ERSSTv5 and EXs 1–3 are high (0.85–0.97) over the periods of January 1997 and January 1999. These results suggest that ERSSTv5 is able to appropriately represent the 1997/98 El Niño even if superobs are reduced to the level of 1877/78, although Niño-3 dips in EX-2 over October–December 1997 (Fig. 11, dotted green). This implies that ERSSTv5 properly resolves the 1877/78 El Niño with the parameter combinations of HF = 3mon and Crit = 10%, HF = 1mon and Crit = 10%, and HF = 3mon and Crit = 20%.

Nevertheless, the analysis in EX-4 (HF = 1mon and Crit = 20%) completely fails to represent the 1997/98 El Niño (Figs. 10e and 11, dotted purple), which is consistent with the same parameter combinations applied to

TABLE 2. Variance ratio (r_i in unit %) of EOTs 1, 2, 3, and 6 as a function of HF = 3mon and HF = 1mon in January 1878. The quantification of r_i is expressed in Eq. (1).

	EOT-1	EOT-2	EOT-3	EOT-6
HF = 3mon	23	7	26	42
HF = 1mon	17	3	15	24

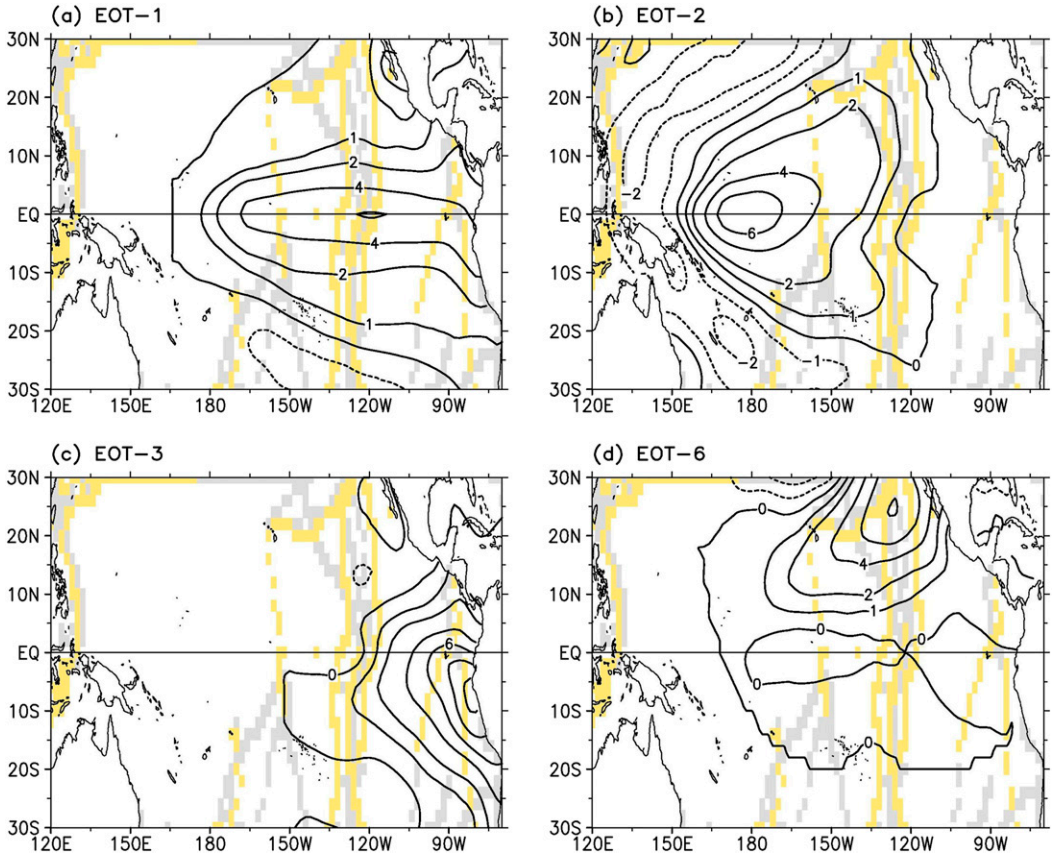

FIG. 9. Dominant four EOTs (contours) used in ERSSTv5 in the Pacific between 30°S and 30°N. (a) EOT-1, (b) EOT-2, (c) EOT-3, and (d) EOT-6. Contours (−2, −1, 0, 1, 2, 4, 6, 8, and 10) represents EOT loading. Yellow shadings represents the grid boxes containing observations in SST reconstruction in January 1878 when HF = 1mon, and gray shading represents additional grid boxes containing observations when HF = 3mon.

1877/78 (Fig. 8d). These results indicate that the parameter selections of HF = 1mon and Crit = 20% indeed create too much spread and artificially reduced ensemble mean values in the 1000-member ensemble and should be discounted as suggested in section 4b and shown in Fig. 3 (solid red) and Fig. 5d.

e. The 1877/78 El Niño strength

After the combined parameters of HF = 1mon and Crit = 20% are excluded, uncertainties in the Niño-3 and Niño-3.4 indices are approximately 0.54° and 0.56°C, respectively, in December 1877 (Table 1; EN = 318). The ERSSTv5 Niño-3 index is approximately 2.93°, or 3.47°C if a 30-yr running climatology is applied. The strength of the 1877/78 El Niño in ERSSTv5 in the Niño-3 region can therefore be expressed as 2.93° ± 0.54°C or 3.47° ± 0.54°C, which is among the strongest El Niño events. As a point of comparison, Niño-3 during 1997/98 El Niño has a strength of 3.23° ± 0.20°C (Table 1). Here, we have selected EN = 318 to examine the Niño indices in ERSSTv5 ensemble and their uncertainty as discussed in the previous sections.

To determine whether one event (expressed as $a_1 \pm b_1$) is stronger than the other one (expressed as $a_2 \pm b_2$), their difference can be assessed by $a_1 - a_2 \pm \sqrt{b_1^2 + b_2^2}$ (Ku 1966), where the a and b terms represent the magnitude and uncertainty of El Niño events, respectively. Applying the formula to the 1877/78 and 1997/98 El Niño events, the difference of the Niño-3 index is approximately −0.30° ± 0.58°C, or 0.24° ± 0.58°C if a 30-yr running climatology is applied. Since the absolute difference (0.30° or 0.24°C) is less than the uncertainty of the difference (0.58°C), the strengths of the 1877/78 and 1997/98 El Niño events are statistically indistinguishable. Likewise, the strengths of the El Niño events quantified by Niño-3 are statistically indistinguishable over 1877/78 and 1982/83. Similarly, the comparison between the 1877/78 and 2015/16 El Niño events shows that the difference in the Niño-3.4 index is approximately −0.26° ± 0.58°C, or 0.39° ± 0.58°C if a 30-yr running climatology is applied to the 1877/78

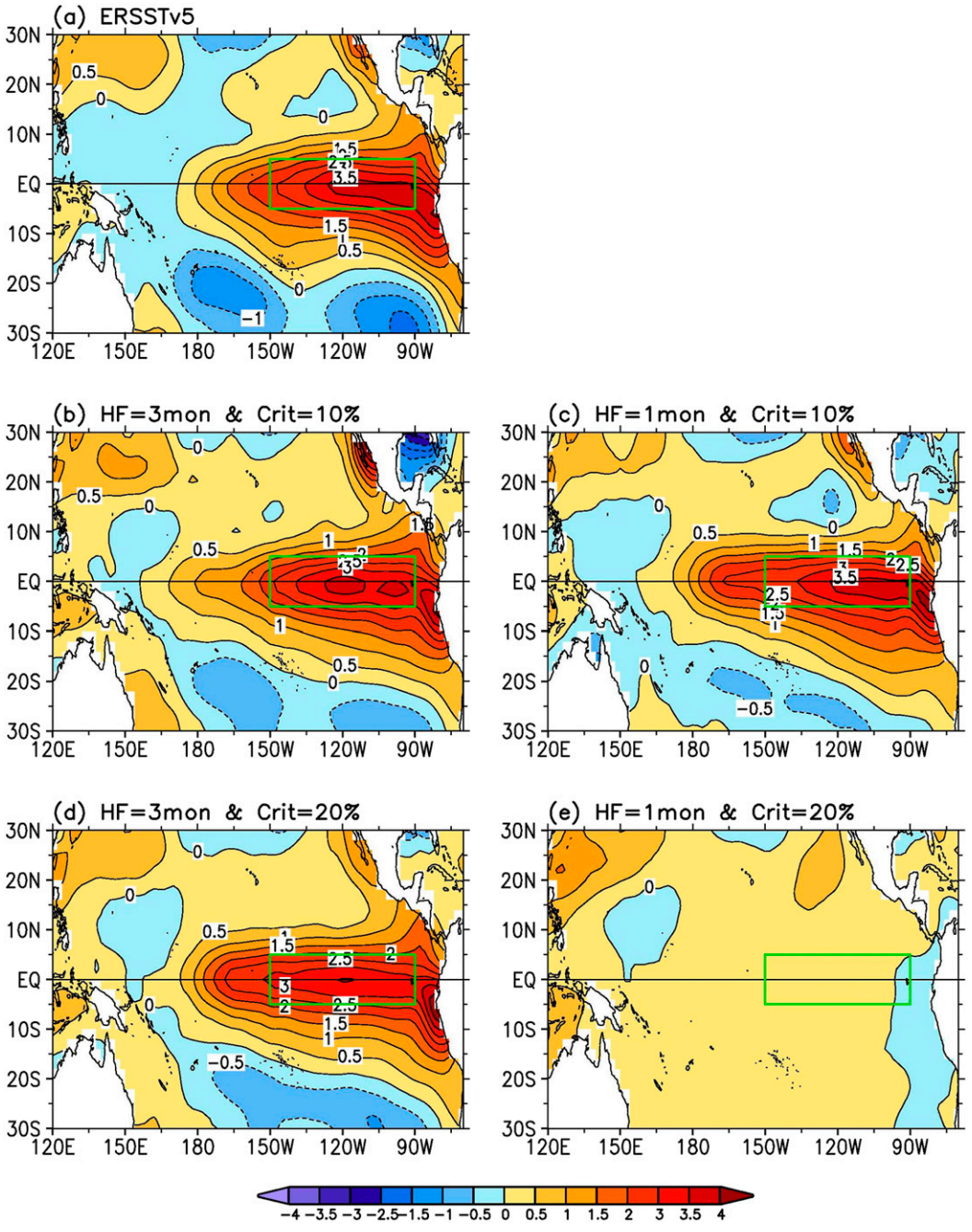

FIG. 10. SSTAs in January 1998 in (a) ERSSTv5 and experiments using (b) HF = 3mon and Crit = 10%, (c) HF = 1mon and Crit = 10%, (d) HF = 3mon and Crit = 20%, and (e) HF = 1mon and Crit = 20%. In these experiments, observations from 1981 to 2017 are reduced by the mask of observations from 1861 to 1897. Correlation coefficients between ERSSTv5 in (a) and these experiments in (b)–(e) are 0.94, 0.93, 0.96, and −0.08, respectively.

event. Therefore, the strengths of the 1877/78 and 2015/16 events are statistically the same too.

These comparisons indicate that the El Niño of 1877/78 is among the strongest, which is consistent with the evidence provided in previous studies using the SOI index, precipitation, and food product and famine record (Singh et al. 2018). However, we are not able to conclude that the El Niño event of 1877/78 is stronger than those of 1997/98, 1982/83, or 2015/16 based on our analysis. What can be concluded is that the El Niño of 1877/78 is among the strongest El Niño events in the entire ERSSTv5 historical record.

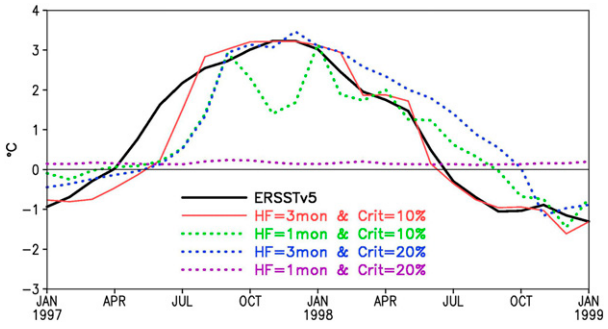

FIG. 11. Niño-3.4 indices in official ERSSTv5 (solid black) and its observation-reduced experiments of HF = 3mon and Crit = 10% and (solid red), HF = 1mon and Crit = 10% (dotted green), HF = 3mon and Crit = 20% (dotted blue), and HF = 1mon and Crit = 20% (dotted purple). Correlation coefficients between these experiments and the official ERSSTv5 are 0.97, 0.86, 0.85, and 0.37, respectively.

5. Conclusions

The ERSSTv5 analysis clearly shows a strong El Niño during 1877/78. The ranking of El Niño strength will vary depending on the SST dataset, the Niño regions examined, and the climatology that is used. Here, we attempt to quantify how strong it was in the SST record using the monthly 2° × 2° ERSSTv5 (Huang et al. 2017). To compare the strength of El Niño events, the uncertainty of the Niño indices should be taken into account (Huang et al. 2016a). To date, the uncertainty has rarely been considered in comparing the strength of El Niño events. In ERSST, the SST uncertainty consists of parametric and reconstruction uncertainties (Huang et al. 2016b, 2020). For a regionally averaged SST such as Niño indices, the parametric uncertainty dominates over the reconstruction uncertainty. A 1000-member ensemble analysis of ERSSTv5 (Huang et al. 2020) is used to quantify the parametric uncertainty of Niño indices, which depends on the 2–7 selections of 28 parameters. Our initial analysis of the 1000-member ensemble shows that the ensemble averaged Niño-3 over 1877/78 is lower (1.8°C) than the value from ERSSTv5 standard run while the uncertainty is large (2.8°C). In contrast, the uncertainty range in the Niño-3 and Niño-3.4 indices during 1982/83, 1997/98, and 2015/16 is much smaller (0.1°–0.2°C).

The reasons for the small Niño-3 index value and large uncertainty among the ensemble members over 1877/78 has been investigated using factor analysis here among the 28 ERSSTv5 parameters. We find two of the 28 parameters are especially critical in representing El Niño events when observational data are sparse. In particular, the selections of 1-month high-frequency filter and 20% EOT acceptance criterion appear to reduce the Niño indices by 0.6°–0.8°C and increase the uncertainty by approximately 1.1°C. By removing these members within the 1000-member ensemble, a reassessment of the data confirms a strong El Niño during 1877/78 (with averaged Niño-3 value of 2.8°C and reduced uncertainty of 0.5°C). However, with these adjustments, the Niño indices and their uncertainty do not change much during 1982/83, 1997/98, and 2015/16, suggesting that the selections of those two parameters do not exert a large influence on the SST reconstruction across the tropical Pacific in the modern era. The reason for a more stable SST reconstruction in the modern era is due to the better observational coverage after the 1960s (80%) than during the 1870s (10%).

The strong 1877/78 El Niño in ERSSTv5 is consistent with independent SOI index derived from sea level pressure measurements in Darwin and Tahiti (Trenberth 1984). This El Niño event in ERSSTv5 is also consistent with the precipitation and temperature proxy data derived from tree rings and coral reefs and from the great famine record in southeastern Asia and Africa (Kiladis and Diaz 1986; Allan et al. 1991; D'Arrigo et al. 2008; Garden 2008; Hao et al. 2010; Räsänen et al. 2016; Singh et al. 2018; Lough et al. 2018). For example, Singh et al. (2018) used the Palmer drought severity index (PDSI) in Asia and demonstrated a record-breaking El Niño during 1877/78. D'Arrigo et al. (2008) used the PDSI in Australia and Lough et al. (2018) used the degree heating month index (DHMI) derived from coral reef in the tropical oceans; both showed a strong El Niño event during 1877/78.

The strong 1877/78 El Niño in ERSSTv5 is consistent with that in HadSST1 (Fig. 2c; dotted blue) (Rayner et al. 2003). The Niño-3 index is approximately 0.5°C lower in HadISST1 than in ERSSTv5 from January 1877 to February 1878, which is in the range of the uncertainty of ERSSTv5 as indicated in Fig. 5d and Table 1. The temporal correlation between ERSSTv5 and HadISST1 Niño-3 indices between January 1877 and January 1879 is high (approximately 0.94). The consistency between the 1997/98 El Niño events in ERSSTv5 and HadSST1 is very good with strong correlations (0.99) between January 1997 and January 1999 (Fig. 2f).

In conclusion, the strength (2.8°–3.5°C) and uncertainty (0.5°C) of the 1877/78 El Niño event are quantified by evaluating the selection of certain parameters in the ERSSTv5 ensemble. The strength of the 1877/78 El Niño appears approximately equal to those during 1982/83, 1997/98, and 2015/16.

Acknowledgments. The authors thank Dr. Todd P. Mitchell and an anonymous reviewer for their comments that have greatly improved our manuscript. The

authors thank Eric Freeman for his help in providing ICOADS R3 data, and thank Vikram Mehta for the discussion at the early stage. The 1000-member ensemble of ERSSTv5 can be accessed at ftp://ftp.ncdc.noaa.gov/pub/data/cmb/ersst/v5/2019.ersstv5.ensemble.

REFERENCES

Aceituno, P., M. Prieto, M. Solari, A. Martínez, G. Poveda, and M. Falvey, 2009: The 1877–1878 El Niño episode: Associated impacts in South America. *Climatic Change*, **92**, 389–416, https://doi.org/10.1007/s10584-008-9470-5.

Allan, R. J., N. Nicholls, P. D. Jones, and I. J. Butterworth, 1991: A further extension of the Tahiti-Darwin SOI, early ENSO events and Darwin pressure. *J. Climate*, **4**, 743–749, https://doi.org/10.1175/1520-0442(1991)004<0743:AFEOTT>2.0.CO;2.

Ashok, K., S. K. Behera, S. A. Rao, H. Weng, and T. Yamagata, 2007: El Niño Modoki and its possible teleconnections. *J. Geophys. Res.*, **112**, C11007, https://doi.org/10.1029/2006JC003798.

——, T. P. Sabin, P. Swapna, and R. G. Murtugudde, 2012: Is a global warming signature emerging in the tropical Pacific? *Geophys. Res. Lett.*, **39**, L02701, https://doi.org/10.1029/2011GL050232.

Barnston, A. G., M. Chelliah, and S. B. Goldenberg, 1997: Documentation of a highly ENSO-related SST region in the equatorial Pacific: Research note. *Atmos.–Ocean*, **35**, 367–383, https://doi.org/10.1080/07055900.1997.9649597.

Cai, W., and Coauthors, 2014: Increasing frequency of extreme El Niño events due to greenhouse warming. *Nat. Climate Change*, **4**, 111–116, https://doi.org/10.1038/nclimate2100.

Capotondi, A., and P. D. Sardeshmukh, 2017: Is El Niño really changing? *Geophys. Res. Lett.*, **44**, 8548–8556, https://doi.org/10.1002/2017GL074515.

Changnon, S. A., 1999: Impacts of 1997–98 El Niño generated weather in the United States. *Bull. Amer. Meteor. Soc.*, **80**, 1819–1827, https://doi.org/10.1175/1520-0477(1999)080<1819:IOENOG>2.0.CO;2.

Curtis, S., and S. Hastenrath, 1999: Long-term trends and forcing mechanisms of circulation and climate in the equatorial Pacific. *J. Climate*, **12**, 1134–1144, https://doi.org/10.1175/1520-0442(1999)012<1134:LTTAFM>2.0.CO;2.

D'Arrigo, R., P. Baker, J. Palmer, K. Anchukaitis, and G. Cook, 2008: Experimental reconstruction of monsoon drought variability for Australasia using tree rings and corals. *Geophys. Res. Lett.*, **35**, L12709, https://doi.org/10.1029/2008GL034393.

Deser, C., A. S. Phillips, and M. A. Alexander, 2010: Twentieth century tropical sea surface temperature trends revisited. *Geophys. Res. Lett.*, **37**, L10701, https://doi.org/10.1029/2010GL043321.

Diaz, H. F., and G. J. McCabe, 1999: A possible connection between the 1878 yellow fever epidemic in the southern United States and the 1877–78 El Niño episode. *Bull. Amer. Meteor. Soc.*, **80**, 21–27, https://doi.org/10.1175/1520-0477(1999)080<0021:APCBTY>2.0.CO;2.

Enfield, D. B., 1988: Is El Niño becoming more common? *Oceanography*, **1**, 23–27, https://doi.org/10.5670/oceanog.1988.04.

Freeman, E., and Coauthors, 2017: ICOADS release 3.0: A major update to the historical marine climate record. *Int. J. Climatol.*, **37**, 2211–2232, https://doi.org/10.1002/joc.4775.

Garden, D., 2008: El Niño, irrigation dams and stopbanks: Examining the repercussions of the 1876-78 El Niño in Australia and New Zealand. *Hist. Meteor.*, **4**, 1–26, http://www.meteohistory.org/2008historyofmeteorology4/1garden.pdf.

Goddard, L., and M. Dilley, 2005: El Niño: Catastrophe or opportunity. *J. Climate*, **18**, 651–665, https://doi.org/10.1175/JCLI-3277.1.

Grove, R. H., 1998: Global impact of the 1789–93 El Niño. *Nature*, **393**, 318–319, https://doi.org/10.1038/30636.

Hao, Z. X., J. Y. Zheng, G. F. Wu, X. Z. Zhang, and Q. S. Ge, 2010: 1876–1878 severe drought in North China: Facts, impacts and climatic background. *Chinese Sci. Bull.*, **55**, 3001–3007, https://doi.org/10.1007/s11434-010-3243-z.

Hu, Z.-Z., A. Kumar, H.-L. Ren, H. Wang, M. L'Heureux, and F.-F. Jin, 2013: Weakened interannual variability in the tropical Pacific Ocean since 2000. *J. Climate*, **26**, 2601–2613, https://doi.org/10.1175/JCLI-D-12-00265.1.

——, ——, B. Jha, and B. Huang, 2020: How much of monthly mean precipitation variability over global land is associated with SST anomalies? *Climate Dyn.*, **54**, 701–712, https://doi.org/10.1007/s00382-019-05023-5.

Huang, B., and Z. Liu, 2001: Temperature trend of the last 40 years in the upper Pacific Ocean. *J. Climate*, **14**, 3738–3750, https://doi.org/10.1175/1520-0442(2001)014<3738:TTOTLY>2.0.CO;2.

——, and Coauthors, 2015: Extended reconstructed sea surface temperature version 4 (ERSST.v4), Part I. Upgrades and intercomparisons. *J. Climate*, **28**, 911–930, https://doi.org/10.1175/JCLI-D-14-00006.1.

——, M. L'Heureux, Z.-Z. Hu, and H.-M. Zhang, 2016a: Ranking the strongest ENSO events while incorporating SST uncertainty. *Geophys. Res. Lett.*, **43**, 9165–9172, https://doi.org/10.1002/2016GL070888.

——, and Coauthors, 2016b: Further exploring and quantifying uncertainties for Extended Reconstructed Sea Surface Temperature (ERSST) version 4 (v4). *J. Climate*, **29**, 3119–3142, https://doi.org/10.1175/JCLI-D-15-0430.1.

——, and Coauthors, 2017: Extended reconstructed sea surface temperature version 5 (ERSSTv5): Upgrades, validations, and intercomparisons. *J. Climate*, **30**, 8179–8205, https://doi.org/10.1175/JCLI-D-16-0836.1.

——, C. Liu, G. Ren, H.-M. Zhang, and L. Zhang, 2019: The role of buoy and Argo observations in two SST analyses in the global and tropical Pacific Oceans. *J. Climate*, **32**, 2517–2535, https://doi.org/10.1175/JCLI-D-18-0368.1.

——, and Coauthors, 2020: Uncertainty estimates for sea surface temperature and land surface air temperature in NOAAGlobalTemp version 5. *J. Climate*, **33**, 1351–1379, https://doi.org/10.1175/JCLI-D-19-0395.1.

Johnson, N. C., 2013: How many ENSO flavors can we distinguish? *J. Climate*, **26**, 4816–4827, https://doi.org/10.1175/JCLI-D-12-00649.1.

Kennedy, J. J., N. A. Rayner, R. O. Smith, D. E. Parker, and M. Saunby, 2011a: Reassessing biases and other uncertainties in sea surface temperature observations measured in situ since 1850: 1. Measurement and sampling uncertainties. *J. Geophys. Res.*, **116**, D14103, https://doi.org/10.1029/2010JD015218.

——, ——, ——, ——, and ——, 2011b: Reassessing biases and other uncertainties in sea surface temperature observations measured in situ since 1850: 2. Biases and homogenization. *J. Geophys. Res.*, **116**, D14104, https://doi.org/10.1029/2010JD015220.

Kent, E., N. A. Rayner, D. I. Berry, M. Saunby, B. I. Moat, J. J. Kennedy, and D. E. Parker, 2013: Global analysis of night marine air temperature and its uncertainty since 1880: The HadNMAT2 data set. *J. Geophys. Res. Atmos.*, **118**, 1281–1298, https://doi.org/10.1002/JGRD.50152.

Kiladis, G. N., and H. F. Diaz, 1986: An analysis of the 1877–78 ENSO episode and comparison with 1982–83. *Mon. Wea. Rev.*, **114**, 1035–1047, https://doi.org/10.1175/1520-0493(1986)114<1035:AAOTEE>2.0.CO;2.

Knutson, T. R., and S. Manabe, 1998: Model assessment of decadal variability and trends in the tropical Pacific Ocean. *J. Climate*, **11**, 2273–2296, https://doi.org/10.1175/1520-0442(1998)011<2273:MAODVA>2.0.CO;2.

Ku, H. H., 1966: Notes on the use of propagation of error formulas. *J. Res. Natl. Bur. Stand.*, **70C**, 263–273, https://doi.org/10.6028/jres.070c.025.

Kumar, A., A. G. Barnston, P. Peng, M. P. Hoerling, and L. Goddard, 2000: Changes in the spread of the variability of the seasonal mean atmospheric states associated with ENSO. *J. Climate*, **13**, 3139–3151, https://doi.org/10.1175/1520-0442(2000)013<3139:CITSOT>2.0.CO;2.

Larkin, N. K., and D. E. Harrison, 2005: On the definition of El Niño and associated seasonal average U.S. weather anomalies. *Geophys. Res. Lett.*, **32**, L13705, https://doi.org/10.1029/2005GL022738.

Latif, M., R. Kleeman, and C. Eckert, 1997: Greenhouse warming, decadal variability, or El Niño? An attempt to understand the anomalous 1990s. *J. Climate*, **10**, 2221–2239, https://doi.org/10.1175/1520-0442(1997)010<2221:GWDVOE>2.0.CO;2.

——, V. A. Semenov, and W. Park, 2015: Super El Niños in response to global warming in a climate model. *Climatic Change*, **132**, 489–500, https://doi.org/10.1007/s10584-015-1439-6.

Lee, T., and M. J. McPhaden, 2010: Increasing intensity of El Niño in the central equatorial Pacific. *Geophys. Res. Lett.*, **37**, L14603, https://doi.org/10.1029/2010GL044007.

L'Heureux, M. L., D. C. Collins, and Z.-Z. Hu, 2013: Linear trends in sea surface temperature of the tropical Pacific Ocean and implications for the El Niño–Southern Oscillation. *Climate Dyn.*, **40**, 1223–1236, https://doi.org/10.1007/s00382-012-1331-2.

——, M. K. Tippett, and A. G. Barnston, 2015: Characterizing ENSO coupled variability and its impact on North American seasonal precipitation and temperature. *J. Climate*, **28**, 4231–4245, https://doi.org/10.1175/JCLI-D-14-00508.1.

Li, X., Z.-Z. Hu, and B. Huang, 2019: Contributions of atmosphere–ocean interaction and low-frequency variation to intensity of strong El Niño events since 1979. *J. Climate*, **32**, 1381–1394, https://doi.org/10.1175/JCLI-D-18-0209.1.

Lough, J. M., K. D. Anderson, and T. P. Hughes, 2018: Increasing thermal stress for tropical coral reefs: 1871–2017. *Sci. Rep.*, **8**, 6079, https://doi.org/10.1038/s41598-018-24530-9.

McGregor, S., A. Timmermann, M. H. England, O. E. Timm, and A. T. Wittenberg, 2013: Inferred changes in El Niño–Southern Oscillation variance over the past six centuries. *Climate Past*, **9**, 2269–2284, https://doi.org/10.5194/cp-9-2269-2013.

Newman, M., S. I. Shin, and M. A. Alexander, 2011: Natural variation in ENSO flavors. *Geophys. Res. Lett.*, **38**, L14705, https://doi.org/10.1029/2011GL047658.

Quinn, W. H., and V. T. Neal, 1995: The historical record of El Niño events. *Climate since A.D. 1500*, R. S. Bradley and P. D. Jones, Eds., Routledge, 623–648.

Rajagopalan, B., and E. Cook, 2000: Spatiotemporal variability of ENSO and SST teleconnections to summer drought over the United States during the twentieth century. *J. Climate*, **13**, 4244–4255, https://doi.org/10.1175/1520-0442(2000)013<4244:SVOEAS>2.0.CO;2.

Räsänen, T. A., V. Lindgren, J. H. A. Guillaume, B. M. Buckley, and M. Kummu, 2016: On the spatial and temporal variability of ENSO precipitation and drought teleconnection in mainland Southeast Asia. *Climate Past*, **12**, 1889–1905, https://doi.org/10.5194/cp-12-1889-2016.

Rayner, N. A., D. E. Parker, E. B. Horton, C. K. Folland, L. V. Alexander, D. P. Rowell, E. C. Kent, and A. Kaplan, 2003: Global analyses of sea surface temperature, sea ice, and night marine air temperature since the late nineteenth century. *J. Geophys. Res.*, **108**, 4407, https://doi.org/10.1029/2002JD002670.

Ropelewski, C. F., and P. D. Jones, 1987: An extension of the Tahiti-Darwin southern oscillation index. *Mon. Wea. Rev.*, **115**, 2161–2165, https://doi.org/10.1175/1520-0493(1987)115<2161:AEOTTS>2.0.CO;2.

Singh, D., R. Seager, B. I. Cook, M. Cane, M. Ting, and E. Cook, 2018: Climate and the global famine of 1876–78. *J. Climate*, **31**, 9445–9467, https://doi.org/10.1175/JCLI-D-18-0159.1.

Smith, T. M., and R. W. Reynolds, 2003: Extended reconstruction of global sea surface temperature based on COADS data (1854–1997). *J. Climate*, **16**, 1495–1510, https://doi.org/10.1175/1520-0442-16.10.1495.

——, and ——, 2004: Improved extended reconstruction of SST (1854–1997). *J. Climate*, **17**, 2466–2477, https://doi.org/10.1175/1520-0442(2004)017<2466:IEROS>2.0.CO;2.

Stevenson, S. L., 2012: Significant changes to ENSO strength and impacts in the twenty-first century: Results from CMIP5. *Geophys. Res. Lett.*, **39**, L17703, https://doi.org/10.1029/2012GL052759.

Takahashi, K., A. Montecinos, K. Goubanova, and B. Dewitte, 2011: ENSO regimes: Reinterpreting the canonical and Modoki El Niño. *Geophys. Res. Lett.*, **38**, L10704, https://doi.org/10.1029/2011GL047364.

Trenberth, K. E., 1984: Signal versus noise in the Southern Oscillation. *Mon. Wea. Rev.*, **112**, 326–332, https://doi.org/10.1175/1520-0493(1984)112<0326:SVNITS>2.0.CO;2.

——, and T. J. Hoar, 1996: The 1990–1995 El Niño–Southern Oscillation event: Longest on record. *Geophys. Res. Lett.*, **23**, 57–60, https://doi.org/10.1029/95GL03602.

van den Dool, H. M., S. Saha, and A. Johansson, 2000: Empirical orthogonal teleconnections. *J. Climate*, **13**, 1421–1435, https://doi.org/10.1175/1520-0442(2000)013<1421:EOT>2.0.CO;2.

Wang, G., W. Cai, B. Gan, L. Wu, A. Santoso, X. Lin, Z. Chen, and M. J. McPhaden, 2017: Continued increase of extreme El Niño frequency long after 1.5°C warming stabilization. *Nat. Climate Change*, **7**, 568–572, https://doi.org/10.1038/nclimate3351.

Wittenberg, A. T., 2015: Low-frequency variations of ENSO. *U.S. CLIVAR Variations*, No. 13, U.S. CLIVAR Project Office, Washington, DC, 26–31, https://usclivar.org/sites/default/files/documents/2015/Variations2015Winter_0.pdf.

Yu, J.-Y., and S. T. Kim, 2013: Identifying the types of major El Niño events since 1870. *Int. J. Climatol.*, **33**, 2105–2112, https://doi.org/10.1002/joc.3575.

Yuan, L., Z. Yu, Z. Xie, Z. Song, and G. Lu, 2009: ENSO signals and their spatial-temporal variation characteristics recorded by the sea-level changes in the northwest Pacific margin during 1965–2005. *Sci. China*, **52D**, 869–882, https://doi.org/10.1007/s11430-009-0072-5.

Zebiak, S. E., and M. A. Cane, 1987: A model El Niño–Southern Oscillation. *Mon. Wea. Rev.*, **115**, 2262–2278, https://doi.org/10.1175/1520-0493(1987)115<2262:AMENO>2.0.CO;2.